

High-Temperature Ferromagnetism in $\text{Si}_{1-x}\text{Mn}_x$ ($x \approx 0.5$) Nonstoichiometric Alloys

V. V. Rylkov^{a,*}, S. N. Nikolaev^a, K. Yu. Chernoglazov^a, B. A. Aronzon^a, K. I. Maslakov^b,
V. V. Tugushev^{a,**}, E. T. Kulatov^c, I. A. Likhachev^a, E. M. Pashaev^a, A. S. Semisalova^b,
N. S. Perov^b, A. B. Granovskii^b, E. A. Gan'shina^b, O. A. Novodvorskii^d,
O. D. Khramova^d, E. V. Khaidukov^d, and V. Ya. Panchenko^d

^a National Research Centre Kurchatov Institute, pl. Kurchatova 1, Moscow, 123182 Russia

* e-mail: vvrylkov@mail.ru

** e-mail: tuvictor@mail.ru

^b Moscow State University, Moscow, 119991 Russia

^c Prokhorov General Physics Institute, Russian Academy of Sciences, ul. Vavilova 38, Moscow, 119991 Russia

^d Institute on Laser and Information Technologies, Russian Academy of Sciences,
Svyatoozerskaya ul. 1, Shatura, Moscow region, 140700 Russia

Received July 12, 2012

It has been found that the Curie temperature ($T_C \sim 300$ K) in nonstoichiometric $\text{Si}_{1-x}\text{Mn}_x$ alloys slightly enriched in Mn ($x \approx 0.52$ – 0.55) in comparison to the stoichiometric manganese monosilicide MnSi becomes about an order of magnitude higher than that in MnSi ($T_C \sim 30$ K). Deviations from stoichiometry lead to a drastic decrease in the density of charge carries (holes), whereas their mobility at about 100 K becomes an order of magnitude higher than the value characteristic of MnSi. The high-temperature ferromagnetism is ascribed to the formation of defects with the localized magnetic moments and by their indirect exchange interaction mediated by the paramagnetic fluctuations of the hole spin density. The existence of defects with the localized magnetic moments in $\text{Si}_{1-x}\text{Mn}_x$ alloys with $x \approx 0.52$ – 0.55 is supported by the results of numerical calculations performed within the framework of the local-density-functional approximation. The increase in the hole mobility in the nonstoichiometric material is attributed to the decay of the Kondo (or spin-polaron) resonances presumably existing in MnSi.

DOI: 10.1134/S0021364012160114

1. The development and studies of semiconductor systems based on Group IV elements, in particular, $\text{Si}_{1-x}\text{Mn}_x$ alloys, attract considerable current interest. Such materials are promising for applications in spintronics as integrated-circuit elements easily incorporated into the existing microelectronic technology [1]. In addition, these alloys exhibit interesting and unusual magnetic characteristics, which cannot be adequately interpreted within the framework of the available theoretical models (see, e.g., [2, 3] and references therein).

In $\text{Si}_{1-x}\text{Mn}_x$ films with $x \approx 0.35$, we have recently observed room-temperature ferromagnetism accompanied by the pronounced anomalous Hall effect [4]. The results were interpreted within the framework of model [3] based on the assumption that the nonstoichiometric material under study forms a semiconducting or semimetallic host with the inclusions containing the higher manganese silicides having the chimney ladder type structure and the composition close to $\text{MnSi}_{1.72-1.75}$ (see [5] and references therein). The stoichiometric silicides of the aforementioned

type are weak band ferromagnets with a relatively low “intrinsic” Curie temperature ($T_C^0 < 50$ K) and clearly pronounced spin fluctuations (paramagnons) at temperatures exceeding T_C^0 . According to the model discussed in [3], deviations from stoichiometry in the host material give rise to defects with magnetic moments more or less localized at uncompensated hybridized orbitals of Si and Mn. It was shown that silicon vacancies could play the role of such defects [5]. The exchange interaction between the magnetic moments of defects mediated by the paramagnons in the host material leads to a significant increase in the “true” Curie temperature T_C in comparison to T_C^0 . The subsequent studies demonstrated that the preparation of well-reproducible magnetic alloys such as $\text{Si}_{1-x}\text{Mn}_x$ ($x \approx 0.35$) is rather problematic owing to the existence of numerous (no less than five) stable higher silicide phases of the chimney ladder type.

In this work, we analyze the magnetic properties of $\text{Si}_{1-x}\text{Mn}_x$ films with $x \approx 0.5$, which are quite different from those studied in [4] and are close to the metallic

manganese monosilicide MnSi. According to the conventional viewpoint, below the Curie temperature ($T_C^0 \approx 29$ K), the stoichiometric compound MnSi is a weak helicoidal band ferromagnet exhibiting strong spin fluctuations in the paramagnetic phase ($T > T_C^0$). These fluctuations determine the specific features of its magnetic and transport characteristics [6, 7]. The fact that the magnetic moment per Mn atom found from the saturation magnetization measured at low temperatures ($\approx 0.4\mu_B/\text{Mn}$ at $T = 1.4$ K) is significantly smaller than the effective magnetic moment $\approx 2.2\mu_B/\text{Mn}$ estimated using the Curie–Weiss behavior of the magnetic susceptibility in the paramagnetic phase [7] is an important reason for this viewpoint. At first glance, in the nonstoichiometric alloys based on manganese monosilicide MnSi, which contain magnetic defects, a significant enhancement of the exchange interaction and the high-temperature ferromagnetic ordering of the magnetic moments of these defects according to the mechanism suggested in [3] implying the Curie temperature $T_C \gg T_C^0$ can be expected by analogy with the related alloys based on the higher silicides of the chimney ladder type. However, a more careful analysis shows that the situation is not so clear because of the possible existence of the Kondo and spin-polaron resonances in stoichiometric MnSi and their decay in $\text{Si}_{1-x}\text{Mn}_x$ nonstoichiometric films. We shall discuss some subtle features of the mechanism suggested in [3] under such conditions after the description of the main results of our investigation.

2. $\text{Si}_{1-x}\text{Mn}_x$ films 55–70 nm thick with different Mn contents ($x = 0.44\text{--}0.6$) were produced by the pulsed laser deposition method using the time-of-flight separation of the deposited particles and with the control of the energy spectrum of ions in the laser erosion plume [8]. The deposition of layers onto the (0001) Al_2O_3 substrate was performed in vacuum (at pressure below 10^{-7} Torr) at 340°C with the deposition rate equal to 1.5 nm/min. The surface roughness of the Si films produced in such a way did not exceed 1 nm. To study the transport characteristics, we produced (using special masks) the $\text{Si}_{1-x}\text{Mn}_x/\text{Al}_2\text{O}_3$ structure in the shape of the Hall cross having the conduction channel with the width $W = 1.2$ mm and the distance between the voltage probes $L = 1.4$ mm. At the same time, to study the structural features of the films and their composition, we prepared the rectangular samples 4.4×5.0 mm in size.

The structural features of the films were studied by X-ray diffraction analysis using a Rigaku SmartLab diffractometer without a monochromator and a diaphragm before the detector. The spectrum of the incident radiation included the characteristic $\text{Cu}K_{\alpha 1}$, $\text{Cu}K_{\alpha 2}$, and $\text{Cu}K_{\beta 1}$ lines. The intensity of the direct beam was as high as 1.5×10^9 pulses/s. The chemical

composition of the films was determined by X-ray photoelectron spectroscopy (XPS) using a Quanters SXM spectrometer. The measurements were performed in a vacuum of about 10^{-8} mbar after cleaning of the film surface for 60 s by argon ions with an energy of 2 kV. The thickness of the removed layer was about 5–10 nm.

The studies of the transport characteristics (conductivity and Hall constant) were performed using an evacuated insert with a superconducting solenoid submerged in a liquid helium Dewar flask operating within the 5–100 K temperature range at magnetic fields up to 2.5 T. The measurements at relatively high temperatures (77–300 K) were carried out inside a liquid nitrogen Dewar. At these temperatures, the magnetic field (≤ 1 T) was generated by an electromagnet. The magnetization of the $\text{Si}_{1-x}\text{Mn}_x$ samples was measured using a VSM Lake Shore 7407 vibrating-sample magnetometer (with the sensitivity no lower than 10^{-5} emu) at applied magnetic field up to 15 kOe within the 90–400 K temperature range. In the course of measurements, the applied magnetic field was oriented along the sample plane.

3. By special experiments with pure (99.9 at %) Mn plates, it was found that an appreciable manifestation of carbon and oxygen in the X-ray photoelectron spectra results from their adsorption at the chemically active surface of the plates even in a relatively high vacuum (about 10^{-8} mbar). Therefore, the XPS studies were used mainly for the analysis of the relative content of silicon and manganese in the $\text{Si}_{1-x}\text{Mn}_x$ films: $y = (1-x)/x$. To calculate the values of y , we used the data reported in [9]. The sample studied in this work was a MnSi single crystal with the surface obtained by its cleavage directly within the vacuum chamber of the spectrometer.

The XPS analysis of the chemical composition of the films allowed us to select for our studies $\text{Si}_{1-x}\text{Mn}_x$ samples with a different manganese content, $x = 1/(1+y) = 0.44\text{--}0.63$. The characteristic parameters of the most interesting samples alongside the results of the transport and magnetic measurements are given in the table. Samples J0806 and J2112 have a remarkable feature: they deviate from the MnSi composition by nearly the same amount toward enrichment and depletion in Si, $\Delta x/x \approx 10\%$. Sample J0504 with the maximum Mn content ($x \approx 0.625$) is the reference sample. It corresponds to Mn_3Si_3 silicide, which exhibits an antiferromagnetic ordering at low carbon content $N_C < 2$ at % [10] and ferromagnetic ordering at $N_C > 2$ at %. The last sample, J0604, is characterized by the ratio of the components close to that in MnSi.

Figure 1 shows the photoelectron spectra of sample J0604 corresponding to $\text{Si}2p$ and $\text{Mn}3p$ lines in comparison with the spectra for a MnSi single crystal reported in [9], as well as with the spectra for the sample with $x \approx 0.55$. We can see that this sample has

Parameters of the $\text{Si}_{1-x}\text{Mn}_x/\text{Al}_2\text{O}_3(0001)$ structures

Sample	Film thickness d , nm	Mn content x	Resistivity ρ_{xx} at $T \approx 300$ K, $\text{m}\Omega \text{ cm}$	Hole density p at $T \approx 100$ K, 10^{21} cm^{-3}	Curie temperature of ferromagnetic phases ¹ T_{C1} (T_{C2}), K
J0806	55	0.44	0.77	4 ²	No ferromagnetism at $T \geq 100$ K
J0604	70	≈ 0.52	0.18	1.5	330
J2112	60	0.55	0.44	2.2	230 (490)
J0504	75	0.625	0.3	15	No ferromagnetism at $T \geq 100$ K

Notes: ¹ Sample J2112 exhibits two ferromagnetic phases.

² Charge carrier density in sample J0806 increases significantly with temperature and becomes as high as $1.2 \times 10^{22} \text{ cm}^{-3}$ at $T \approx 300$ K.

a small deficit of Si in comparison to MnSi. For this sample, the estimated y value is lower than unity by several percent and corresponds to $x \approx 0.52$.

The X-ray diffraction results for the $\text{Si}_{1-x}\text{Mn}_x/\text{Al}_2\text{O}_3(0001)$ structure with $x \approx 0.52$ (sample J0604) are illustrated in the inset of Fig. 1. The X-ray diffraction pattern contains intense reflection peaks coming from $\text{Al}_2\text{O}_3(0006)$ for the $\text{Cu}K_{\alpha 1}$, $\text{Cu}K_{\alpha 2}$, and $\text{Cu}K_{\beta 1}$ lines. In addition to these peaks, the presented pattern exhibits a broad peak at an angle $2\theta = 44.43^\circ$ related to the $\text{Cu}K_{\alpha}$ line to the MnSi(100) film. The structural perfection of the film is described by such an integral characteristic as the FWHM of the peak in the rocking curve (FWHM_ω). For the film under study, the FWHM_ω parameter at $2\theta = 44.43^\circ$ is $\Delta\omega \approx 0.4^\circ$, whereas the FWHM_ω value for the single-crystalline film of the same thickness should be about 250 seconds of arc. Such a broad peak observed for the film is a signature of a pronounced mosaicity of this structure as well as of a large number of structural defects.

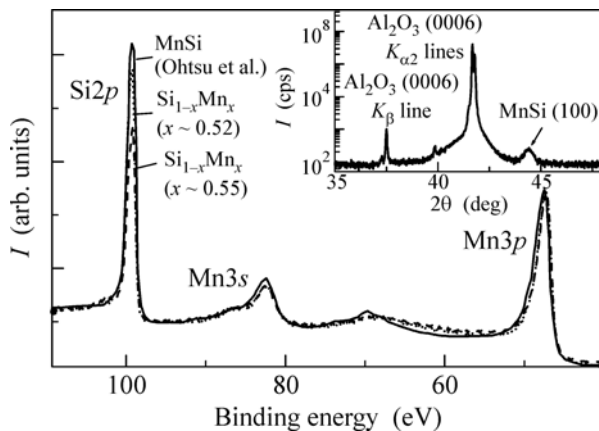


Fig. 1. Photoelectron spectra corresponding to Si2p and Mn3p lines for $\text{Si}_{1-x}\text{Mn}_x/\text{Al}_2\text{O}_3$ structures with $x \approx 0.52$ and 0.55 produced after the surface cleaning by argon ions for 60 s in comparison with similar spectra for the MnSi single crystal reported in [9]. The X-ray diffraction pattern for the $\text{Si}_{1-x}\text{Mn}_x/\text{Al}_2\text{O}_3$ structure with $x \approx 0.52$ is shown in the inset.

Figure 2 shows the temperature dependence of the resistivity $\rho_{xx}(T)$ for the structures listed in the table. The minimum resistivity is observed for sample J0604 having the smallest deviation from stoichiometry and hence the lowest content of structural defects. However, the resistivity of this sample decreases only by a factor of about 1.3 when the temperature drops from 300 to 5 K. This is much less than in the case of MnSi, for which this factor is as large as 40–100 [11, 12]. In addition, at $T < T_C^0 \approx 29$ K, the behavior of MnSi is characterized by the range of a relatively steep decrease in the resistivity. At the same time, the samples with a small excess of Mn ($x \approx 0.52$ and 0.55) exhibit another tendency in the behavior of $\rho_{xx}(T)$: the resistivity tends to saturation below 30 K (Fig. 2). In addition, sample J0504 ($x \approx 0.625$) exhibits the range of a steep decrease in $\rho_{xx}(T)$ below 40 K, which is also observed in the case of pure Mn_5Si_3 films [10]. This is a clear indication that our samples have only a small content of residual (uncontrolled) carbon impurities.

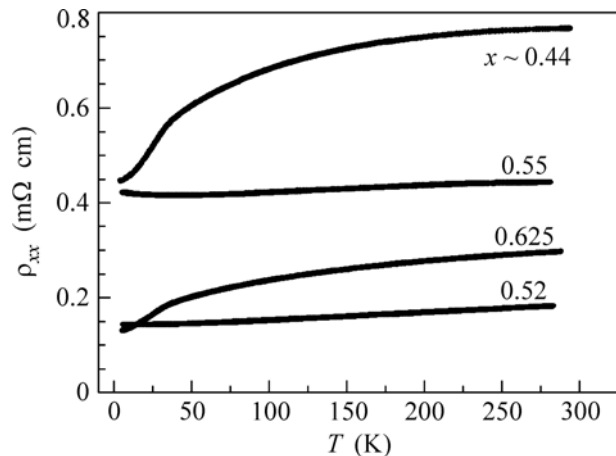


Fig. 2. Temperature dependence of the resistivity for $\text{Si}_{1-x}\text{Mn}_x/\text{Al}_2\text{O}_3$ structures with different Mn contents ($x \approx 0.44, 0.52, 0.55,$ and 0.625).

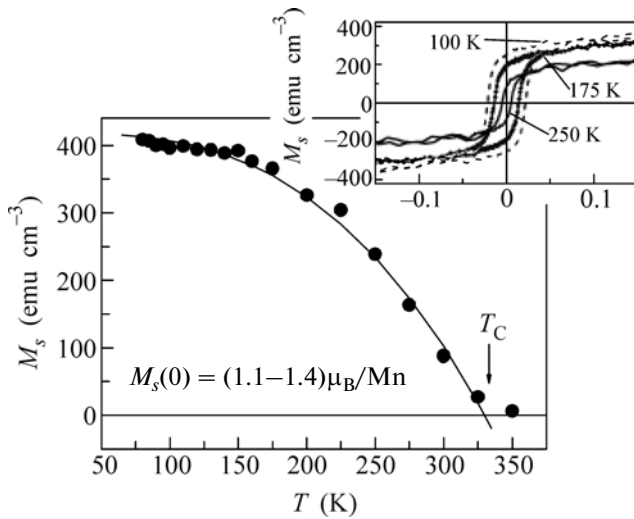


Fig. 3. Temperature dependence of the magnetization for the $\text{Si}_{1-x}\text{Mn}_x/\text{Al}_2\text{O}_3$ structure J0604 ($x \approx 0.52$). Experimental points and (solid curve) the fit to function (1) with the parameters $n = 1.4$, $T_C = 330$ K, and $T_C^0 = 30$ K. The inset shows the magnetic field dependence of the magnetization of this sample at $T = 100, 175, \text{ and } 250$ K.

Below, we demonstrate that, under such conditions, the magnetic properties of the samples with a small excess of Mn ($x \approx 0.52$ and 0.55) differ drastically from those of MnSi single crystals.

For the sample with the lowest excess of Mn ($x \approx 0.52$), where only a single magnetic phase is observed, the temperature dependence of the saturation magnetization $M_s(T)$ is shown in Fig. 3. (In the sample with $x \approx 0.55$, the $M_s(T)$ curve exhibits a clearly pronounced kink suggesting the existence of two magnetic phases with different Curie temperatures. To estimate T_C of these phases, the $M_s(T)$ curve was fitted by the often used simplified Brillouin function of the form $M_s(T) = M_s(0)[1 - (T/T_C)^n]$ (usually $n = 1.5-2.5$). In this sample, we find $T_{C1} \approx 230$ K and $T_{C2} \approx 490$ K; see the table.) In such a case, an accurate fit is assured through the use of the function $M_s(T)$ determined in [4] within the framework of the model proposed in [3] for the $\text{Si}_{1-x}\text{Mn}_x$ system with $x \approx 0.35$:

$$M_s(T) \approx M_s(0) \left\{ 1 - \left[\frac{T(T - T_C^0)}{T_C(T_C - T_C^0)} \right]^n \right\}, \quad (1)$$

where $T_C^0 \approx 30$ K is the “intrinsic” Curie temperature for MnSi. Using Eq. (1) for the sample with $x \approx 0.52$, we find $T_C \approx 330$ K, that is, the value an order of magnitude higher than in the case of MnSi. It is also important that the magnetic field dependence of the magnetization in this sample exhibits a hysteresis up to $T \approx 250$ K (see inset of Fig. 3). Such a hysteresis is not observed for the helicoidal magnet MnSi. The magnetic moments per Mn ion estimated for samples J0604 ($x = 0.52$) and J2112 ($x = 0.55$) based on the sat-

uration magnetization are equal to $(1.1-1.4)\mu_B$ and $0.74\mu_B$, respectively (the estimate from below, $1.1\mu_B$, is obtained for the density of $\text{Si}_{1-x}\text{Mn}_x$ film equal to that of monosilicide MnSi). At the same time, for stoichiometric MnSi, the magnetic moment per Mn atom in the temperature range corresponding to the ferromagnetic state turns out to be much smaller ($\approx 0.4\mu_B$) [6]. This can be attributed to defects with local magnetic moments arising in our samples.

In sample J0806 ($x \approx 0.44$) with the deficit of Mn, as well as in sample J0504 ($x \approx 0.625$) with the big excess of Mn, we did not observe any ferromagnetism in the temperature range $T \geq 100$ K. This follows not only from the magnetization measurements but also from the studies of the anomalous Hall effect discussed below.

We recall that the Hall resistivity R_H in magnetic materials is a sum of the normal and anomalous components of the Hall effect

$$R_H d = \rho_H = R_0 B + R_s M, \quad (2)$$

where d is the thickness of the layer made of a magnetic material; R_0 is the constant characterizing the normal Hall effect stemming from the Lorentz force and proportional to the magnetic field B ; $R_s \propto (\rho_{xx})^\alpha$ is the constant characterizing the anomalous Hall effect, which is proportional to magnetization M ; and exponent α depends on the mechanism of the anomalous Hall effect: $\alpha = 1$ for the skew scattering and $\alpha = 2$ for the intrinsic and side-jump mechanisms [13].

The studies of the anomalous Hall effect in disordered magnetic semiconductors play a key role in the identification of the ferromagnetic state in these materials [1, 13], although the anomalous Hall effect is a rather complicated quantum phenomenon, the nature of which is still under discussion [13]. One of the main causes underlying such “popularity” is the fact that, for all currently known mechanisms of the anomalous Hall effect, its observation is a clear signature of the existence of spin-polarized charge carriers in the system, in contrast to the observation of the magnetization [14, 15]. In other words, the anomalous Hall effect characterizes the magnetic ordering only in such part of the magnetic subsystem which mainly determines the spin polarization of the charge carriers and is the most important for possible applications of magnetic semiconductors in spintronics.

The measured B dependence of the Hall resistivity at different temperatures for the samples, the parameters of which are listed in the table, is illustrated in Fig. 4. In the samples with a small excess of manganese ($x \approx 0.52$ and 0.55), we observe a clearly pronounced anomalous Hall effect dominating over the normal component of the Hall effect (Fig. 4a). In these samples, the anomalous Hall effect at $T = 6$ K exhibits a hysteretic behavior (curves 1 and 2 in Fig. 4a). It is also interesting (see Fig. 4) that the mag-

nitude of the anomalous Hall effect in sample J2112 significantly (by about a factor of two) decreases at 197 K (curve 2'), whereas in sample J0604 with the chemical composition closest to MnSi, the value of the anomalous component of the Hall effect remains nearly the same in this temperature range (cf. curves 1 and 1' in Fig. 4a for $T = 6$ and 197 K, respectively). Moreover, the anomalous component of the Hall resistivity ρ_H^a turns out to be approximately a factor of five higher than in the earlier studied $\text{Si}_{1-x}\text{Mn}_x$ films with $x \approx 0.35$ [4]. Finally, let us draw attention to the fact that the anomalous Hall effect in all samples has a positive sign, whereas the anomalous Hall effect in crystalline MnSi is negative [11, 12]. This demonstrates an appreciable difference in the properties between the films under study and the crystalline silicide MnSi.

Let us recall that two phases with quite different Curie temperatures were observed in the sample with $x \approx 0.55$. A significant change in the magnitude of the anomalous Hall effect in this sample within the 6–200 K temperature range indicates the percolative nature of its conductivity. The high-temperature magnetic phase with $T_{C2} \approx 490$ K has only nonzero magnetization but does not have conductivity since it is “discontinuous.” In other words, for sample J2112, the anomalous Hall effect is determined by the low-temperature phase with $T_{C1} \approx 230$ K. It is natural to attribute the drop in the anomalous Hall effect by several times at $T \approx 200$ K to the transition of this phase to the paramagnetic state. In sample J0604, we observe only one phase with $T_C \approx 330$ K. Therefore, the absence of an appreciable change in the anomalous Hall effect in the 6–200 K temperature range is quite natural. This conclusion is supported by the Hall effect measurements performed at room temperature (see the top inset of Fig. 4a). We can see that the anomalous Hall effect in this sample is observed only for sample J0604 ($x \approx 0.52$). It is important to note that the results of the anomalous Hall effect studies correlate well with the measurements of the temperature and frequency dependences of the magneto-optic Kerr effect (the results of these measurements will be published elsewhere alongside the results of the numerical calculations; see below). In particular, these measurements demonstrate that magneto-optic properties in the sample with $x \approx 0.55$ are mainly determined by the phase with $T_{C1} \approx 230$ K.

The Hall resistivity of sample J0806 ($x \approx 0.44$) with the deficit on Mn and sample J0504 ($x \approx 0.625$) with the pronounced excess of Mn behaves linearly above 100 K (see Fig. 4b). The anomalous Hall effect in sample J0806 ($x \approx 0.44$) manifests itself at the liquid helium temperature (curve 3). However, the Hall resistivity behaves linearly even at 64 K (curve 3'). In sample J0504 ($x \approx 0.625$), a slight anomaly in the Hall effect is observed at 66 K (curve 4). It completely disappears at 144 K (line 4').

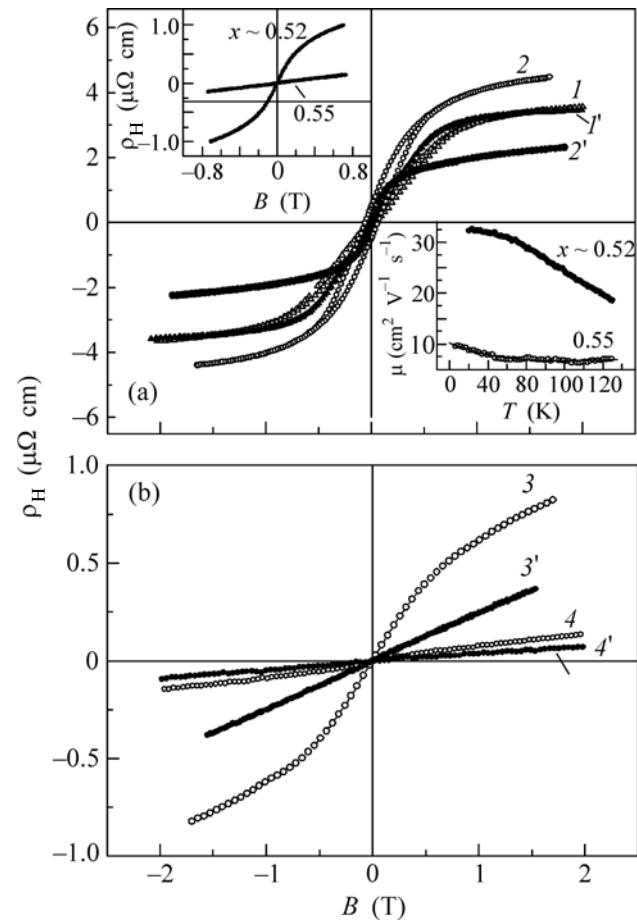


Fig. 4. (a) Magnetic field dependence of the Hall resistivity ρ_H for sample J0604 ($x \approx 0.52$) at $T = (1)$ 6 and $(1')$ 197 K and for sample J2112 ($x \approx 0.55$) at $T = (2)$ 6 and $(2')$ 197 K. The top inset shows $\rho_H(B)$ curves at room temperature for the samples with $x \approx 0.52$ and 0.55. The bottom inset shows the temperature dependence of the charge carrier mobility μ in these samples. (b) $\rho_H(B)$ curves for sample J0806 ($x \approx 0.44$) at $T = (3)$ 5 and $(3')$ 64 K and for sample J0504 ($x \approx 0.625$) at $T = (4)$ 66 and $(4')$ 144 K.

To get a deeper insight into the features of the transport characteristics and magnetism of $\text{Si}_{1-x}\text{Mn}_x$ samples under study, we analyzed in addition the temperature behavior of the normal component of the Hall effect to get information on the density of charge carriers and their mobility. According to Eq. (2), at a high applied magnetic field under conditions of saturated magnetization, $R_H(B)$ is a linear function and its behavior is determined by the normal component of the Hall effect. In our case, it has a positive sign (Fig. 4), which corresponds to the hole conductivity similar to the case of MnSi [11, 12].

The magnitude of the normal component of the Hall effect was determined by the extrapolation of the linear $R_H(B)$ dependence in fields higher than 1.2 T. Using the slope of these curves (factor R_0), we determined the hole density p in the samples; its values at

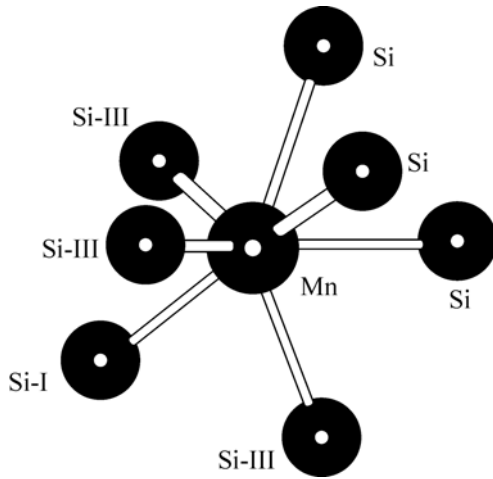


Fig. 5. Partial image of the supercell with a Mn atom, around which Si vacancies are created, and its seven nearest-neighbor Si atoms. A single vacancy is created at the Si-I site ($x \approx 0.51$). Three vacancies are created at three Si-III sites ($x \approx 0.52$). Four vacancies are created at one Si-I site and three Si-III sites ($x \approx 0.53$).

$T = 100$ K are given in the table. It is remarkable that the charge carrier density (1.5×10^{21} and $2.2 \times 10^{21} \text{ cm}^{-3}$) is minimal in the samples with a small excess of manganese: J0604 ($x \approx 0.52$) and J2112 ($x \approx 0.55$). At the same time, the p values for these samples is significantly smaller (by more than an order of magnitude) than in MnSi, where $p \approx 3.78 \times 10^{22} \text{ cm}^{-3}$ at $T = 300$ K and $p \approx 8.5 \times 10^{22} \text{ cm}^{-3}$ at $T \leq 30$ K [11, 12]. At first glance, the mobility of charge carriers under such conditions should be only lower than that in MnSi, as usually takes place in degenerate semiconductors, if we introduce there an appreciable number of defects. However, in our case, we have encountered the opposite situation.

In the bottom inset of Fig. 4a, we demonstrate the temperature dependence of the charge carrier mobility μ for $\text{Si}_{1-x}\text{Mn}_x$ samples with $x \approx 0.52$ and 0.55 . In sample J0604 ($x \approx 0.52$), the value of μ remains nearly unchanged below 60 K and equals $31\text{--}32.5 \text{ cm}^2/\text{V s}$. In contrast to that, in MnSi single crystals, the mobility at $T = 60$ K is only about $2 \text{ cm}^2/\text{V s}$ and it grows up to $28 \text{ cm}^2/\text{V s}$ at $T = 4.2$ K [16]; that is, the μ value in MnSi is lower than that in the case of the disordered $\text{Si}_{1-x}\text{Mn}_x$ film ($x \approx 0.52$). Even in sample J2112 with $x \approx 0.55$, where the disorder is so pronounced that the phase separation effects manifest themselves, we have mobility $\mu \approx 7 \text{ cm}^2/\text{V s}$ at 60 K, which is appreciably higher than that in MnSi.

Thus, the aforementioned data demonstrate that the lattice constant a in the disordered $\text{Si}_{1-x}\text{Mn}_x$ layers with $x \approx 0.52$ coincides with that for MnSi. However, the Curie temperature for $\text{Si}_{1-x}\text{Mn}_x$ layers with $x \approx 0.52$ is an order of magnitude higher than that in the case of MnSi. It is also surprising that, despite the

significant structural disorder of the produced films, they exhibit also a much higher mobility of charge carriers.

4. We attribute the high-temperature ferromagnetism observed in $\text{Si}_{1-x}\text{Mn}_x$ films with a slight excess of Mn ($x \approx 0.52$) to two factors: (i) the formation of defects with the local magnetic moments and (ii) the exchange interaction between these local magnetic moments according to the mechanism discussed in [3]. The existence of defects with local magnetic moments is confirmed by numerical calculations performed within the framework of the density functional theory using the full-potential augmented plane wave method (FLAPW) [17]. The exchange-correlation effects were taken into account through the use of the generalized gradient approximation (GGA) [18]. The electron structure calculations were performed using supercells $(2 \times 2 \times 2)a^3$ containing from 60 to 64 atoms. The positions of all atoms in the supercell were optimized. The band energies and electron wavefunctions were calculated taking into account the spin-orbit interaction. Integration in k space was performed by the method of tetrahedra over about 340 k points in the irreducible part of the Brillouin zone.

The band calculations for $\text{Si}_{1-x}\text{Mn}_x$ with the excess of Mn, which was modeled by vacancies in the Si sublattice (Fig. 5), demonstrate that the average magnetic moment per Mn atom in the ground state at $x \approx 0.51\text{--}0.53$ is $m_{\text{Mn}} = (1.1\text{--}1.5)\mu_B$. This value far exceeds $m_{\text{Mn}} \approx 0.4\mu_B$ characteristic of stoichiometric MnSi [6] and agrees well with the experimental data (see Fig. 3). Note that the peak values can be as large as $1.99\mu_B$, $2.58\mu_B$, and $3.32\mu_B$ at $x \approx 0.51$, 0.52 , and 0.53 , respectively, for the Mn positions located near the Si vacancies. Figure 6 shows the electron density of states calculated for ferromagnetic phases of $\text{Si}_{1-x}\text{Mn}_x$ ($x \approx 0.51$, 0.52 , and 0.53). It is noteworthy that all three cases exhibit a half-metallic ferromagnetic state with an integer total magnetic moment per supercell; that is, the Fermi level in the spin-majority subband falls within the narrow band gap (semiconducting state), whereas the Fermi level in the spin-minority subband crosses the bands (metallic state). There is also an interesting feature of the density of states below the Fermi level at $x \approx 0.52$ (Fig. 6b), where two closely located energy bands are split from the top of the valence band in the spin-majority subband. These bands give a peak in the local density of states and contain two spin-up electrons. The mechanisms underlying the formation of this peak, as well as the calculation of the optical and magneto-optical characteristics of $\text{Si}_{1-x}\text{Mn}_x$ with $x \approx 0.55$, will be published later.

In addition, for $\text{Si}_{1-x}\text{Mn}_x$ ($x \approx 0.52$), we performed the calculations in order to study the effects of the substitution of a Mn atom for an Si atom and of the introduction of one interstitial Mn atom. In this case, to describe the Mn concentrations under study, we

needed to have $(1 \times 2 \times 3)a^3$ and $(1 \times 1 \times 3)a^3$ supercells, respectively. The calculations demonstrated that the results for both cases (substitution and introduction) are inconsistent with the experiment: at the substitution of a Mn atom for an Si atom, the average magnetic moment per Mn atom is $m_{\text{Mn}} = 0.84\mu_{\text{B}}$, whereas at introduction, it equals $0.34\mu_{\text{B}}$. In general, both cases are characterized by the ferrimagnetic ordering rather than the ferromagnetic one, whereas the introduced Mn atom turns out to be “magnetically dead” ($m_{\text{Mn}} = 0.09\mu_{\text{B}}$) and the Mn atom appearing as a result of substitution has a large ($m_{\text{Mn}} = -2.08\mu_{\text{B}}$) local magnetic moment antiparallel to those of the other Mn atoms.

Let us now return to the interpretation of the nature of the high-temperature ferromagnetism in nonstoichiometric $\text{Si}_{1-x}\text{Mn}_x$ films ($x \approx 0.5$) within the framework of the model suggested in [3]. The unambiguous interpretation of the magnetic ordering mechanism in stoichiometric MnSi based on the scheme described in [6] was recently criticized in [16, 19]. In particular, comprehensively analyzing the experimental data on the temperature and magnetic field dependences of the resistivity and the electron paramagnetic resonance data, the authors of [16] proposed an explanation of the nature of magnetism in stoichiometric MnSi within the framework of a model more complicated than that discussed in [6]. Such a model assumes the existence of two interacting components of the spin density (“band” and “localized” ones). The authors of [16, 19] suggested the hypothesis that the strong antiferromagnetic interaction of these components leads to the formation of the local regions with the short-range magnetic order, the so-called spin polarons. In our opinion, no less viable is the conjecture on the formation of the Kondo-type state since we are dealing with a metallic material with a sufficiently high charge carrier (hole) density. Both of these hypotheses explain the small value of the effective magnetic moment at Mn at low temperatures and qualitatively agree with the experimental data [7] suggesting a serious cooling-induced transformation of the electron spectrum of the system in the paramagnetic phase (below 50–60 K, but in any case above the intrinsic Curie temperature). Such transformation can be accompanied by the appearance of Kondo or spin-polaron resonances. This should lead to a significant decrease in the charge carrier mobility. It is not quite clear to what extent the existence of such resonances modifies the transition to the long-range ferromagnetic order [6] in stoichiometric MnSi, but this problem lies beyond the scope of this work.

In our opinion, the more important problems concern the existence of the Kondo or spin-polaron resonances in the nonstoichiometric $\text{Si}_{1-x}\text{Mn}_x$ ($x \approx 0.5$) films under study in the high-temperature range (above 100 K) and the possible modification of the mechanism underlying the high-temperature ferro-

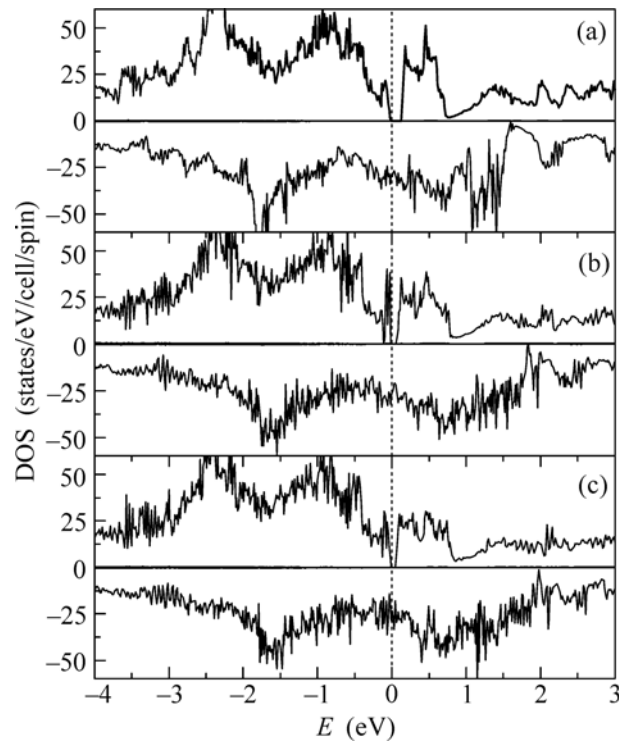


Fig. 6. Spin-polarized electron densities of states for $\text{Si}_{1-x}\text{Mn}_x$ with excess Mn at $x \approx 0.51$ (a), 0.52 (b), and 0.53 (c). The solid curves are total densities of states. The dashed line is the Fermi level from which the energy is measured.

magnetism [3]. It was shown above that the magnetic defects arise in the nonstoichiometric $\text{Si}_{1-x}\text{Mn}_x$ ($x \approx 0.5$) films even at a small excess of Mn ($x \leq 0.55$). At the same time, the hole density in such material decreases by more than an order of magnitude in comparison to that in MnSi single crystals, whereas the Curie temperature begins to exceed 300 K. It is quite surprising that, in spite of an appreciable imperfection of $\text{Si}_{1-x}\text{Mn}_x$ films even at $x = 0.52$, which is revealed by the X-ray diffraction data (the width of the rocking curve $\Delta\omega = 0.4^\circ$ at $2\theta = 44.43^\circ$), their hole mobility $\mu = (20\text{--}32.5) \text{ cm}^2/\text{V s}$ within the 5–150 K temperature range turns out to be much higher than that in MnSi single crystals, where $\mu \approx 2 \text{ cm}^2/\text{V s}$ at $T = 60 \text{ K}$ [16]. We interpret such features in terms of the decay of the Kondo or spin-polaron resonances in the nonstoichiometric $\text{Si}_{1-x}\text{Mn}_x$ ($x \approx 0.5$) films. Such a decay seems to occur owing to the lowering of the hole density simultaneously with the enhanced effect of their scattering by the magnetic defects. Note that the existence of such resonances in stoichiometric MnSi leads to a significant increase in the effective mass of the charge carriers (up to $17m_0$ at $T = 10 \text{ K}$ [20]). Thus, we still do not see any reasons coming from the available experimental data for a serious modification of the model suggested in [3] to interpret the high-tempera-

ture ferromagnetism in the nonstoichiometric $\text{Si}_{1-x}\text{Mn}_x$ ($x \approx 0.5$) films.

In conclusion, we note that, comparing the calculated values of the effective magnetic moment per Mn atom with the experimental data (see Fig. 3), it is necessary to take into account the tendency toward the formation of antiferromagnetic manganese silicide Mn_5Si_3 in $\text{Si}_{1-x}\text{Mn}_x$ ($x \approx 0.5$) films [21]. The contribution of this phase to the magnetization is linear with respect to the applied magnetic field and should be subtracted when we analyze the ferromagnetic component of the magnetization. For this reason, the effective magnetic moments presented for the sample with $x \approx 0.55$ can be underestimated with respect to the calculated values.

The work was supported by the Russian Foundation for Basic Research (project nos. 10-02-00698, 10-02-00118, 10-07-00492, 11-07-12063, 11-02-12200, 11-07-12050, and 11-02-92478) and the Russian Ministry of Education and Science (state contract nos. 07.514.12.4033 and 16.513.11.3088).

REFERENCES

1. S. Zhou and H. Schmidt, *Materials* **3**, 5054 (2010).
2. A. F. Orlov, A. B. Granovsky, L. A. Balagurov, et al., *J. Exp. Theor. Phys.* **109**, 602 (2009).
3. V. N. Men'shov, V. V. Tugushev, and S. Caprara, *Phys. Rev. B* **83**, 035201 (2011); V. N. Men'shov and V. V. Tugushev, *J. Exp. Theor. Phys.* **113**, 121 (2011).
4. B. A. Aronzon, V. V. Rylkov, S. N. Nikolaev, et al., *Phys. Rev. B* **84**, 075209 (2011); S. N. Nikolaev, B. A. Aronzon, V. V. Rylkov, et al., *JETP Lett.* **89**, 603 (2009).
5. S. Caprara, E. Kulatov, and V. V. Tugushev, *Eur. Phys. J. B* **85**, 149 (2012).
6. T. Moriya, *Spin Fluctuations in Itinerant Electron Magnetism* (Springer, Berlin, 1985).
7. S. M. Stishov and A. E. Petrova, *Phys. Usp.* **54**, 1117 (2011).
8. E. V. Khaidukov, O. A. Novodvorsky, V. V. Rocheva, et al., *Tech. Phys. Lett.* **37**, 69 (2011); A. A. Lotin, O. A. Novodvorsky, E. V. Khaidukov, et al., *Semiconductors* **44**, 246 (2010); O. A. Novodvorsky, A. A. Lotin, and E. V. Khaidukov, Patent RF on Useful Model No. 89906, Byull. No. 35 (2009).
9. N. Ohtsu, M. Oku, A. Nomura, et al., *Appl. Surf. Sci.* **254**, 3288 (2008).
10. C. Sürgers, M. Gajdzik, G. Fischer, et al., *Phys. Rev. B* **68**, 174423 (2003); B. Gopalakrishnan, C. Sürgers, R. Montbrun, et al., *Phys. Rev. B* **77**, 104414 (2008).
11. M. Lee, Y. Onose, Y. Tokura, and N. P. Ong, *Phys. Rev. B* **75**, 172403 (2007); M. Lee, W. Kang, Y. Onose, et al., *Phys. Rev. Lett.* **102**, 186601 (2009).
12. A. Neubauer, C. Pfleiderer, R. Ritz, et al., *Physica B* **404**, 3163 (2009).
13. N. Nagaosa, J. Sinova, S. Onoda, et al., *Rev. Mod. Phys.* **82**, 1539 (2010).
14. T. Dietl, in *Modern Aspects of Spin Physics*, Lecture Notes in Physics, Ed. by W. Potz, J. Fabian, and U. Hohenester, Vol. 712 (Springer, Berlin, Heidelberg, 2007), p. 1.
15. V. V. Rylkov, B. A. Aronzon, Yu. A. Danilov, et al., *J. Exp. Theor. Phys.* **100**, 742 (2005).
16. S. V. Demishev, A. V. Semeno, A. V. Bogach, et al., *JETP Lett.* **93**, 213 (2011); S. V. Demishev, V. V. Glushkov, I. I. Lobanova, et al., *Phys. Rev. B* **85**, 045131 (2012).
17. P. Blaha, K. Schwarz, G. K. H. Madsen, et al., *WIEN2k, An Augmented Plane Wave+Local Orbitals Program for Calculating Crystal Properties* (Karlheinz Schwarz, Techn. Univ., Wien, Austria, 2001).
18. J. P. Perdew, S. Burke, and M. Ernzerhof, *Phys. Rev. Lett.* **77**, 3865 (1996).
19. V. G. Storchak, J. H. Brewer, R. L. Lichti, et al., *Phys. Rev. B* **83**, 140404(R) (2011).
20. F. P. Mena, D. van der Marel, A. Damascelli, et al., *Phys. Rev. B* **67**, 241101(R) (2003).
21. A. B. Gokhale and R. Abbaschian, *Bull. Alloy Phase Diagr.* **11**, 468 (1990).

Translated by K. Kugel